# Modelling ultrasonic laboratory measurements of the saturation dependence of elastic modulus: new insights and implications for wave propagation mechanisms.

Kelvin Amalokwu[1,2,*], Giorgos Papageorgiou[3], Mark Chapman[3] and Angus I. Best[1]

[1]National Oceanography Centre, University of Southampton Waterfront Campus, European Way, Southampton, SO14 3ZH, United Kingdom.

[2]National Oceanography Centre Southampton, University of Southampton, European Way, Southampton, SO14 3ZH, United Kingdom.

[3]University of Edinburgh School of Geosciences Grant Institute, the King's Building West Mains Road Edinburgh, United Kingdom.

[*]Now at the University of Texas at Austin, Jackson School of Geosciences, Austin, Texas, USA.

## 1. Abstract

Seismic time-lapse techniques are a valuable tool used to estimate the mobilization and distribution of stored $CO_2$ in depleted reservoirs. The success of these techniques depends on knowing the seismic properties of partially saturated rocks with accuracy. It is commonplace to use controlled laboratory-scale experiments to determine how the fluid content impacts on their properties. In this work, we measure the ultrasonic P- and S-wave velocities of a set of synthetic sandstones of about 30% porosity. Using an accurate method, we span the entire saturation range of an air-water system. We show that the rocks' elastic behaviour is consistent with patchy saturation and squirt flow models but observe a discontinuity at around 90% gas saturation which can be interpreted in two very different ways. In one interpretation the responsible mechanism is frequency-dependent squirt-flow that occurs in narrow pores that are preferentially saturated. An equally plausible mechanism is the change of the mobile fluid in the pores once they are wetted. Extrapolated to seismic frequencies, our results imply that the seismic properties of rocks may be affected by the wetting effect with an impact on the interpretation of field data but would potentially be unaffected by the squirt flow effect. This provides strong motivation to conduct laboratory-scale experiments with partially saturated samples at lower frequency or, ideally, a range of frequencies in the seismo-acoustic range.

## 2. Introduction

Effective remote seismic monitoring of geological $CO_2$ storage reservoirs for carbon capture and storage (CCS) projects depends on a thorough understanding of the physics associated with wave propagation in rocks saturated with multiple fluids. Model-based approaches help ensure the injected $CO_2$ is accurately interpreted as being trapped within the reservoir, and could also help optimise injection locations, rates and therefore storage. It has been noted that $CO_2$ distribution in the pore space plays an important role in the monitoring process (Eid *et al.*, 2015) and more generally, the contrast between the acoustic properties and densities of oil, brine and $CO_2$ is exploited in monitoring applications of seismic data (Arts *et al.*, 2004, Chadwick *et al.*, 2010, Ghosh *et al.*, 2015), (Toms *et al.*, 2007). However, flow in porous media is controlled by wettability and pore-scale capillary pressure effects (Krevor *et al.*, 2015, Zhang *et al.*, 2016) but these concepts are often neglected in most wave propagation theories used in interpretation of CO2 reservoir time-lapse data.

Models based on physical properties that can relate seismic attributes to $CO_2$ saturation are valuable because they provide a generally applicable framework rather than having to resort to empirical relations. This creates a need for experimental data that can be used to calibrate/validate these models. In general, seismic wave velocity and attenuation are properties that are known to be sensitive to fluid in the pores and this fact has been used to determine and quantify the fluid content in reservoirs (Domenico, 1976, Murphy, 1982, Murphy, 1984, Winkler and Nur, 1982, Winkler and Murphy, 1995). Furthermore, fluid-saturated rocks exhibit frequency-dependent behaviour due to wave-induced fluid flow (Biot, 1956, Chapman *et al.*, 2002, Murphy, 1982, White, 1975). The dispersion arises from unrelaxed wave-induced fluid pressures and is accompanied by seismic attenuation.

Measurements of elastic properties of rocks span a wide range of frequencies, as such; extrapolation of results from one frequency range to another requires an understanding of the mechanisms responsible (Paffenholz and Burkhardt, 1989). Also, the associated frequency-dependence could further be exploited for better saturation estimation either through direct analysis of frequency-dependent effects (Castagna *et al.*, 2003, Wu *et al.*, 2014), or reconciling laboratory measurements to calibrate theoretical models for seismic data interpretation (Gist, 1994, Lei and Xue, 2009). Different physical mechanisms with different characteristic frequencies have been proposed to account for this but there is still no general consensus as to which mechanisms dominate (Müller *et al.*, 2010, Murphy *et al.*, 1986). Controlled laboratory-scale experiments are helpful in understanding the mechanisms associated with multiphase saturation effects on seismic properties and can serve as key calibration tools for the theoretical models (Lei and Xue, 2009, Nakagawa *et al.*, 2013).

Laboratory-scale experimental results on $CO_2$ saturation effects on seismic properties have been interpreted generally using the idea of patchy saturation with a non-Reuss averaged fluid moduli in Gassmann's equations (e.g., Lebedev *et al.*, 2013, Shi *et al.*, 2007) or White's model (e.g., Lei and Xue, 2009, Nakagawa *et al.*, 2013). This is also the case with many partial-gas saturation laboratory experiments in the literature. The model does not always give a good fit to the data, with the moduli usually underestimated. This discrepancy is usually attributed to additional wave-induced fluid related mechanisms not accounted for in these models (e.g., Amalokwu *et al.*, 2016, Carcione *et al.*, 2003, Falcon-Suarez *et al.*, 2016, Nakagawa *et al.*, 2013). It has long been recognised and/or suggested that other mechanisms might be at play and that multiple mechanisms might be required to obtain a better fit between laboratory-scale measurements and theoretical modelling (e.g., Gist, 1994, Wulff and Burkhardt, 1997). However, the data from $CO_2$ experiments does not lend itself well to understanding the saturation-related mechanisms because important saturation

points/intervals are missing due to experimental limitations, as many laboratory $CO_2$ experiments only cover ranges between 0 – 60 % $CO_2$ saturation. The modelling is then done based on these data points, missing the effects of saturation at higher values of the gaseous phase (or $CO_2$) saturation even though there is evidence of multiphase saturation effects at these saturations (Goertz and Knight, 1998, Mavko and Nolen-Hoeksema, 1994, Wulff and Burkhardt, 1997). Also, the uncertainty in accurately determining the saturation state in $CO_2$ experiments complicates the interpretation of the experimental data as saturation has to be estimated from CT scans (e.g., Nakagawa *et al.*, 2013) or resistivity tomography (e.g., Falcon-Suarez *et al.*, 2016). Since in terms of the physics, the wave-induced fluid flow mechanisms in less difficult multiphase experiments are the same as in the case of $CO_2$/brine, a good compromise is to investigate these mechanisms using experiments done with air and water which have an easier control on saturation than those using $CO_2$-brine fluid systems.

A limited number of works have attempted to quantify these effects in order to adequately model the entire saturation dependence using theoretical models (Gist, 1994, Wulff and Burkhardt, 1997), and some have taken a more qualitative approach (e.g., Goertz and Knight, 1998, Mavko and Nolen-Hoeksema, 1994). However, these are very limited and mostly have similar interpretations of the mechanisms, namely, stiffening due to preferential stiffening of the cracks, or due to patchy saturation. Gist (1994) concluded that in order to model satisfactorily the data of Gregory (1976), both the gas-patch model of White (1975) and the squirt flow mechanism need to be considered. However, the heuristic model presented by Gist (1994) accounted for the bulk modulus dispersion due to local flow by assuming shear modulus dispersion was the same as bulk modulus dispersion, an assumption that is not necessarily valid (see Chapman *et al.*, 2002). Aside from the fact that there is limited adequate theoretical interpretation of multiphase laboratory data, the theoretical mechanisms that have been proposed disappear at low frequencies used in seismic field surveys.

Here, we model the effects of saturation from dry to full water saturation by combining different mechanisms. The results show that the interpretation is not unique as different combinations of mechanisms can attain a fit to the experimental data. A major finding of this study is that not all the mechanisms disappear at lower frequencies and this could have important implications for fluid substitution in practice.

## 3. Methods

**Sample Description and Experimental setup**

The samples used in this study were synthetic silica cemented clean sandstones with a mineral composition of almost entirely quartz grains (Tillotson *et al.*, 2014, Tillotson *et al.*, 2012). These experiments were originally designed to study the effects of water saturation on fracture-induced anisotropy. The samples were made from a mixture of sand, kaolinite, and aqueous sodium silicate gel, using a process well documented by Tillotson *et al.* (2012). Results from three samples are presented in this study. There are two cylindrical samples of 5 cm diameter and approximately 2 cm thickness, one blank (non-fractured), and the other containing penny-shaped fractures aligned at $90^o$ to the fracture normal (Figure 1). The fractures in the $90^o$ fractured sample are not expected to affect the results as we expect the response from the crack parallel direction to show no effects due to the fractures except for an increase in rock porosity (e.g. Chapman, 2003, Thomsen, 1995). The third sample used in this study was an octagonal-shaped prism with flat sides of approximately 25 mm made using the same method as the cylindrical samples (see Tillotson *et al.*, 2014).

**Figure 1.** Octagonal, blank and 90° fractured rock samples respectively (from left to right).

Firstly, the rocks were oven-dried at about 40 °C for about 48 hours, and then placed under vacuum until a pressure $10^{-4}$ Pa was achieved, which ensured the rocks were completely dry. Measurements were taken for this vacuum-dried condition. Partial water saturation was then achieved using the method described by Amalokwu *et al.* (2014), which is summarised here. The rocks were placed in an atmosphere of known relatively humidity (RH) for about two weeks for the cylindrical samples and about 4 week for the octagonal sample, until they had reached equilibrium (Amalokwu *et al.*, 2014, Amalokwu *et al.*, 2015a). This method is known to give a more homogeneous distribution of water saturation compared to other methods such as drainage and imbibition, and has been used in other studies (e.g. King *et al.*, 2000, Papamichos *et al.*, 1997, Schmitt *et al.*, 1994).

Controlled relative humidity (RH) was achieved using aqueous saturated salt solutions. Greenspan (1977) gave a range of salt solutions that would maintain a given RH at a particular temperature. The salts used and their approximate RH values (at 20°C laboratory temperature) were Magnesium Nitrate (54%), Ammonium Sulphate (82%), Sodium Carbonate Decahydrate (92%), and Potassium Sulphate (98%) respectively, giving four different $S_w$ values. The maximum water saturation achieved using this method was about 0.4

for the all three rock samples (Amalokwu *et al.*, 2014, Amalokwu *et al.*, 2015a). The rocks were then dried and fully saturated with water using the methods described above. In order to achieve higher water saturation values, a 'modified' drainage method was used which involved wrapping the samples in plastic ("cling") film after each drainage process. The wrapped samples were then placed in a desiccator containing the 98% RH solution, sealed (not vacuum sealed) and left for a minimum of 48 hours. The plastic film (and also the high RH atmosphere) prevents further air/water drainage, thus allowing capillary re-distribution over the length of time left to equilibrate ($\geq$ 48 hours). This was done to minimise effects of heterogeneous saturation distribution caused by drainage (Cadoret *et al.*, 1995, Knight *et al.*, 1998).

To achieve full water saturation, the samples were oven-dried again at about 40 $^{o}$C for about 48 hours, and then placed under vacuum until a pressure $10^{-4}$ Pa was achieved. The samples were then saturated with distilled, deionised and de-aired water under vacuum, and then pressurised to 7 MPa for at least 24 hours until the pressure equilibrates for several hours, ensuring full water saturation (see McCann and Sothcott, 1992).

Velocity and attenuation for the cylindrical samples (blank and 90 degree fractured) were measured using the pulse-reflection method (see Best *et al.*, 2007, McCann and Sothcott, 1992). The velocity for the octagonal sample was measured using a bench-top pulse transmission system (see Amalokwu *et al.*, 2015a, Tillotson *et al.*, 2014).

### 4. Experimental results

We present results for the cylindrical samples at an effective pressure of 40 MPa and a single frequency of 650 kHz obtained from Fourier analysis of broadband signals, to accuracies of $\pm$ 0.3% for the velocities and $\pm$ 0.2 dB/cm for the attenuation coefficient (see McCann and

Sothcott, 1992). Velocity results for the octagonal sample are presented at a single frequency of 500 kHz, to an accuracy of $\pm 0.6\%$ (see Tillotson *et al.*, 2014).

**Velocities**

Elastic wave velocities were measured as a function of water saturation ($S_w$) in all three rock samples.

In the blank sample (Figure 2a), $V_p$ remains roughly constant between $S_w = 0$ and $S_w \approx 0.03$, followed by a sharp increase at $S_w \approx 0.1$, decreasing slightly at $S_w \approx 0.2$. There is a more significant decrease in $V_p$ at $S_w \approx 0.4$, followed by a sharp increase at $S_w \approx 0.5$ and then gradual increments between $S_w \approx 0.7$ and $S_w = 1.0$, with a maximum velocity at $S_w = 1.0$. In the $90^o$ fractured sample, we see a similar behaviour to the blank sample. We see a sharp increase in $V_p$ (Figure 2a) at $S_w \approx 0.13$, followed by subsequent declines at $S_w \approx 0.3$ and $S_w \approx 0.4$, followed by a sharp increase at $S_w \approx 0.6$, stays fairly constant between $S_w \approx 0.7$ and $S_w \approx 0.9$, then decreases slightly at $S_w = 1.0$.
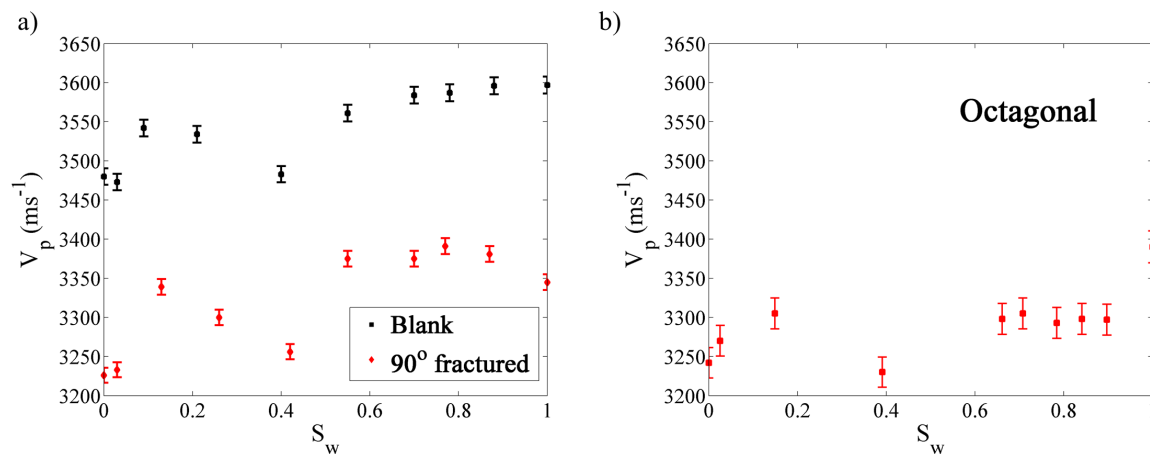


**Figure 2.** $V_p$ versus $S_w$ for (a) the blank and $90^o$ fractured rocks and (b) for the octagonal sample. Figure 2b after Amalokwu *et al.* (2015a).

In the octagonal sample (Figure 2b), we only use measurements in the plane-parallel direction as the rock is anisotropic due to layering, however, similar trends are observed for the other

directions relative to the layering (see Amalokwu *et al.*, 2015a). The general P-wave velocity versus $S_w$ trend is similar to that observed in the cylindrical samples which is an increase in P-wave velocity with increasing $S_w$ apart from a decrease at $S_w \approx 0.40$, the highest velocity occurring at $S_w = 1.0$.

These results are in general agreement with published ultrasonic data (e.g., Gregory, 1976, Marion and Jizba, 1992, Murphy, 1984).

**Moduli**

In order to remove the ambiguity due to the bulk density effect of fluid saturation and to better understand the effect of water saturation on the stiffness of the rocks, we have computed the bulk modulus for both cylindrical samples as we only measured shear wave velocities for these samples (Amalokwu *et al.*, 2015b), and the P-wave modulus for the octagonal sample.
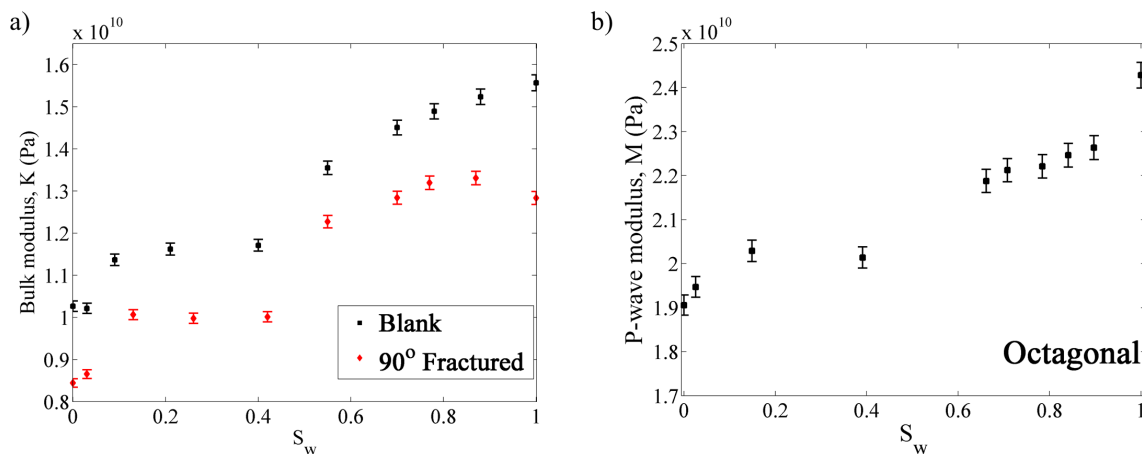


**Figure 3.** (a) Bulk modulus versus $S_w$ for the blank and 90$^o$ fractured rocks. (b) P-wave modulus versus $S_w$ for the octagonal sample (after Amalokwu *et al.*, 2015a).

The moduli in all three rocks show similar behaviour (Figure 3). The moduli stay fairly constant between $S_w = 0$ and $S_w \approx 0.03$, with an increase at $S_w \approx 0.1$, 0.13 and 0.15 for the blank, 90$^o$ fractured and octagonal samples, respectively. The moduli then stay fairly constant

until $S_w \approx 0.4$ in all three samples, after which there is a steady increase until full water saturation, except in the 90° fractured sample where there appears to be a slight drop in modulus.

**Attenuation**

We only present the P-wave attenuation ($Q_p^{-1}$) values for the cylindrical samples as these are the only results we attempt to model. We did not measure attenuation in the octagonal samples.

In the blank sample (Figure 4a), between $S_w$ of $0 - 0.8$, $Q_p^{-1}$ increased steadily as water saturation increased, reaching a maximum at $S_w \approx 0.4$, after which $Q_p^{-1}$ decreased as $S_w$ increased, reaching a minimum at $S_w = 1$. These results are broadly in agreement with previously published experimental observations for non-fractured rocks (Murphy, 1982, Winkler and Nur, 1982).
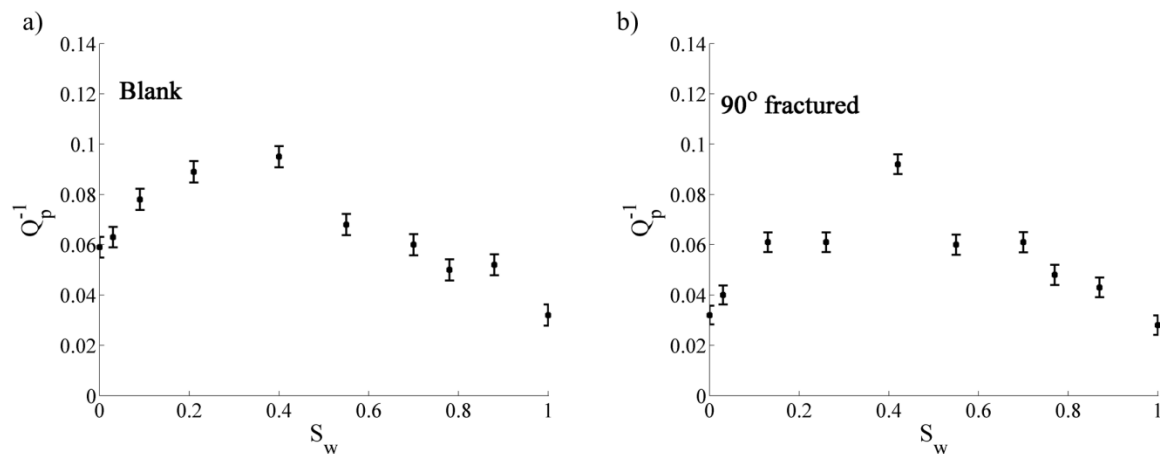


**Figure 4.** $Q_p^{-1}$ versus $S_w$ for (a) the blank rock (b) 90° fractured rock (after Amalokwu et al. 2014).

In the 90° fractured sample (Figure 4b) the trend is similar to that seen in the blank sample. $Q_p^{-1}$ increases steadily between $S_w = 0$ to a maximum at $S_w \approx 0.4$, then begins to decrease steadily as $S_w$ increases, falling to a minimum at $S_w = 1$.

## 5. Theory

Inspection of the data reveals that the partially saturated bulk modulus behaves differently to the Gassmann-Wood prediction. We propose to use two sets of different mechanisms to explain the bulk behaviour at different saturation ranges in a similar spirit to, for example, Mavko and Nolen-Hoeksema (1994) and Wulff and Burkhardt (1997).

As a basis for the modelling we use the well-established models of Gassmann (1951) and White (1975). However, we find neither of these models can explain the rock stiffening at full saturation nor the discontinuity in the bulk modulus observed at $S_w \approx 0.1$ previously noted in Mavko and Nolen-Hoeksema (1994) and Wulff and Burkhardt (1997), and has also been described in Johnson *et al.* (1971). Here we attribute the stiffening at full saturation to the squirt flow mechanism and use the model of Papageorgiou and Chapman (2015) to model it.

The discontinuity can equally well be described by an un-even saturation of the pore space as shown in Papageorgiou and Chapman (2015) or by a discontinuous pressure change in the pore space constituting a new modelling approach.

**Discontinuous pressure change (a wet-Gassmann model)**

It has been noted in the literature (Carcione *et al.*, 2004, Santos *et al.*, 1990) that the existence of capillary pressure affects the elasticity of a partially saturated matrix. If we assume a water-wet porous medium, we can describe the effective fluid saturating the pores with an effective fluid pressure given by the volumetric average:

$$\Delta P = S_w \, \Delta P_w + (1 - S_w) \, \Delta P_{nw}, \tag{1}$$

where $S_w$ is the wetting fluid saturation and $\Delta P_w, \Delta P_{nw}$ are the variations of the wetting and non-wetting fluid pressures respectively. The fluid volume of the effective fluid is the sum of the wetting and non-wetting fluid volumes so the effective fluid modulus $K$ can be calculated as:

$$\frac{\Delta P}{K} = S_w \frac{\Delta P_w}{K_w} + (1 - S_w)\frac{\Delta P_{nw}}{K_{nw}}. \tag{2}$$

This expression leads to Wood's law if $\Delta P_w = \Delta P_{nw}$ but if the pressure variations of the wetting and non-wetting phases are related via a capillary equation, which we can write with the aid of a dimensionless parameter q,

$$\Delta P_{nw} = q \frac{K_{nw}}{K_w} \Delta P_w, \tag{3}$$

so that changes in capillary pressure $C$ are given by

$$\Delta C = \Delta P_{nw} - \Delta P_w = (q \frac{K_{nw}}{K_w} - 1)\Delta P_w, \tag{4}$$

where $1 < q < \frac{K_w}{K_{nw}}$.

In Papageorgiou *et al.* (2016), the coefficient $q$ was found to affect the fluid modulus $K$ in a way that resembles the empirical Brie *et al.* (1995) model. Note that the effective fluid can have a discontinuous rather than uniform change in its pressure.

In this effective medium theory the elastic behaviour of the rock is different if the rock is in wetted or unwetted states. Since we assume an effective fluid in the pore space, a discontinuous effective fluid pressure is needed to account for the transition between the two states. For low water saturation, the effective fluid pressure is that of the non-wetting fluid pressure. This holds up to some critical saturation $S_0$ where the pore space becomes wetted.

For saturations greater than $S_0$ the wetting fluid is the mobile fluid and the effective fluid pressure sharply changes to that of the wetting fluid. This amounts to describing this effective pressure as

$$\Delta P = \begin{cases} \Delta P_{nw}, & if \quad S_w < S_0 \\ \Delta P_w, & if \quad S_w \geq S_0 \end{cases} \tag{5}$$

Because of this discontinuous change, the capillary equation (3) yields a discontinuous effective fluid modulus if combined with equation (2). The discontinuity occurs when $q < \frac{K_w}{K_{nw}}$ at $S_0$ and the fluid modulus is, explicitly:

$$K = \begin{cases} \dfrac{q\, K_{nw}}{S_w + q\,(1 - S_w)}, & S_w < S_0 \\[3mm] \dfrac{K_w}{S_w + q\,(1 - S_w)}, & S_w \geq S_0 \end{cases} \tag{6}$$

This effective fluid modulus can be used in Gassmann's formula instead of the Wood average to obtain a "wet-Gassmann" equation where the wetting effect occurs at a critical saturation $S_0$.

**Squirt model**

In an alternative approach, the partially saturated bulk modulus has a discontinuity at a critical saturation $S_0$ due to an uneven distribution of the wetting fluid in the pore space. In this picture, the rock is modelled on an idealised pore network consisting of spherical pores and ellipsoidal microcracks. The discontinuity occurs because the compliant inclusions (microcracks) become saturated before the spherical ones (pores). To rigorously implement this, we revisit some of the results in Papageorgiou and Chapman (2015) where two different

fluid moduli are used for each type of inclusion. The fluid modulus here labelled $K_-$ corresponds to microcracks

$$\frac{1}{K_-} = \frac{S_w^c}{K_w} + \frac{1 - S_w^c}{K_{nw}} \qquad (7)$$

and the one labelled $K_+$ to pores

$$\frac{1}{K_+} = \frac{S_w^p}{K_w} + \frac{1 - S_w^p}{K_{nw}} \qquad (8)$$

The two moduli are Wood's averages but in this approach different saturation fractions $S_w^p$, $S_w^c$ are used for pores and microcracks respectively. These are related to the observed overall saturation $S_w$ of the sample by means of the definition of the crack fraction $c_f$ (see Endres and Knight, 1997) representing the volume ratio of the microcracks to the total porosity. Volume is conserved if

$$S_w = c_f\, S_w^c + (1 - c_f)\, S_w^p. \qquad (9)$$

Note that if $S_w^p = S_w^c = S_w$ this reduces to the model of Chapman (2002) with a Wood's averaged fluid modulus. On the other extreme, assuming that the microcracks become fully saturated when a critical saturation $S_o$ is reached introduces a discontinuity. This amounts to taking the microcrack and pore saturations as a function of the total saturation as follows

$$S_w^p = \begin{cases} S_w \dfrac{1 - c_f/S_0}{1 - c_f}, & S_w < S_0 \\ \dfrac{S_w - c_f}{1 - c_f}, & S_w \geq S_0 \end{cases} \qquad (10)$$

$$S_w^c = \begin{cases} S_w/S_0, & S_w < S_0 \\ 1, & S_w \geq S_0 \end{cases} \qquad (11)$$

The dispersive bulk modulus of Papageorgiou and Chapman (2015) is used to model the behaviour of the rock at intermediate saturations. The critical saturation together with an arbitrary scaling $a$ of the characteristic time-scale

$$\tau = a \, \tau_0$$

are the two fitting parameters while the rest of the parameters unique to this model are calibrated to match the rock behaviour at 0% and 100% saturation.

## 6. Modelling approach and results

As we noted, inspection of the data reveals that the partially saturated rock behaves differently to what is predicted by the Gassmann-Wood model. On the one hand, there is evidence for patchy dispersion from the shape of the attenuation and bulk modulus curves so we use the model of White (1975) to model this effect. On the other hand, the water saturated rock appears stiffer than Gassmann's prediction due to squirt flow and to model this we use Chapman's (2002) model in the formulation of Papageorgiou and Chapman (2015).

But as far as the discontinuous jump is concerned, both the wet-Gassmann and the squirt models provide reasonable explanations of the mechanisms involved. We compare them by adopting the following two modelling strategies:

16

- In 'case 1' the discontinuity in the bulk modulus is attributed to an uneven saturation between microcracks and pores in what we labelled 'squirt model'. The dispersion due to patchy saturation is accounted for by White (1975).

- In 'case 2' the wet-Gassmann effect is responsible for the discontinuity. The 'squirt model' is then used with homogeneous saturation and is the mechanism responsible for the stiffening at full saturation. Dispersion due to patches is accounted for by White (1975).

In both cases, the squirt model and White's model are the common denominators but the fitting parameters of all models comprising each case (time-scale of squirt flow, patch size etc) need to be fitted since their relative strengths are expected to be different in each case.

In terms of fitting to the data we will only describe in detail the process for the blank sample but the results for rest of the samples follow accordingly. The modelling parameters are given in Tables 1 and 2. For both cases, we take the model fitting parameters that give the best fit at each step and then use those as the starting point in a nonlinear damped least-squares optimisation to obtain the best fitting parameters (Table 2) for the complete saturation modelling plots. It should be pointed out that the starting parameters are similar to the optimised parameters.

In both Case 1 and Case 2, we only fit the model to the measured saturation-dependent bulk modulus, and then the predicted attenuation from the model is compared to the measured attenuation. In essence, we do not fit the attenuation data.

| Rock/Fluid properties | Blank | 90 | Octagonal |
|---|---|---|---|
| Grain bulk modulus | 38 GPa | 38 GPa | 38 GPa |
| Grain shear modulus | 44 Gpa | 44 Gpa | 44 Gpa |

| Grain Density | 2590 | 2590 | 2590 |
|---|---|---|---|
| Porosity | 30.40% | 31.70% | 30.00% |
| Permeability | 40.7 mD | 18.1 mD | 21 mD |
| Gas (air) bulk modulus | 0.0001GPa | | |
| Gas (air) density | 1.2 Kg/m3 | | |
| Water bulk modulus | 2.25 Gpa | | |
| Water density | 1000 Kg/m$^3$ | | |

**Table 1.** Material properties of the rocks and fluid.

**Case 1**

The first case we will explore is conceptually similar to interpretations presented in the literature where the pore space of the rock is considered to consist of thin cracks and more equant pores, which saturate preferentially (e.g., Endres and Knight, 1991, Mavko and Nolen-Hoeksema, 1994, Walsh, 1995). We consider two different mechanisms to explain the saturation dependence of the elastic properties - squirt effects due to the presence of microcracks and patchy effects due to mesoscopic saturation heterogeneities. The squirt effect dominates at lower saturations and essentially leads to a stiffening of the frame depending whether there is enough time for wave-induced fluid flow equilibration (frequency-dependence).

To capture the squirt effect, we use the model of Papageorgiou and Chapman (2015) while the model of White (1975) is used to account for the mesoscopic fluid effect. When the measured moduli for the blank sample are compared to Gassmann's predictions (Figure 5a), we see Gassmann's equation under-predicts the bulk modulus for both full water saturation and most values of $S_w$, and this misfit is attributed to dispersion effects (Mavko and Nolen-

Hoeksema, 1994, Murphy *et al.*, 1986, Murphy, 1984, Murphy, 1985, Winkler, 1985). Firstly, using the squirt model, we pick a critical saturation $S_0$ which indicates the saturation where the microcracks are fully saturated. We picked the saturation at which the jump-discontinuity occurred in the data as $S_0$ which was at $S_w \approx 0.1$ for the blank sample. The microcrack density was then fitted in order to give the desired dispersion at full water saturation ($S_w = 1.0$) and the magnitude of the jump is fitted using the parameter $a$ (see squirt model description) (Figure 5b).
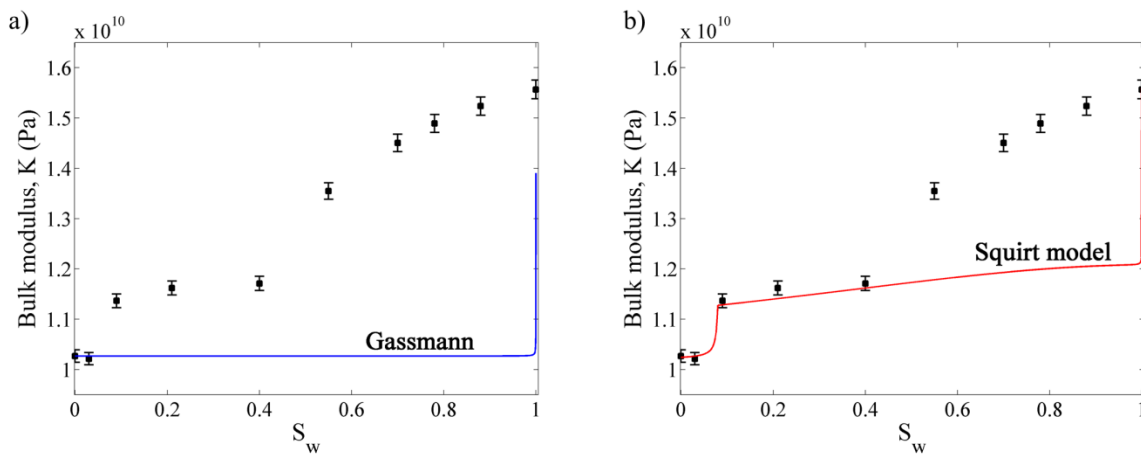


**Figure 5.** Measured bulk modulus for the blank rock compared to (a) Gassmann's model and (b) Squirt model.

The squirt model does not capture the dispersion for partial water saturation values of $S_w > 0.5$. Following a similar concept by (Winkler, 1985), the residual dispersion would be the difference between the measured data and the model (squirt in this case) prediction. We then attribute this dispersion to be due to patchy saturation. A simple yet elegant way to model dispersion and attenuation due to patchy saturation was presented by White (1975). The model only predicts dispersion (and attenuation) to be due to presence of gas patches and is otherwise consistent with Gassmann's predictions at full saturation (no gas patches) (Figure 6a). So the low frequency limit of White's model is consistent with Gassmann's predictions. We then take the difference between the high-frequency White and its low-frequency limit

(Gassmann) as the dispersion due to patchy saturation and fit this to the residuals from the squirt model as shown in Figure 6b. Note the dispersion (or residual) at full saturation is zero as no dispersion is predicted in the absence of gas patches.
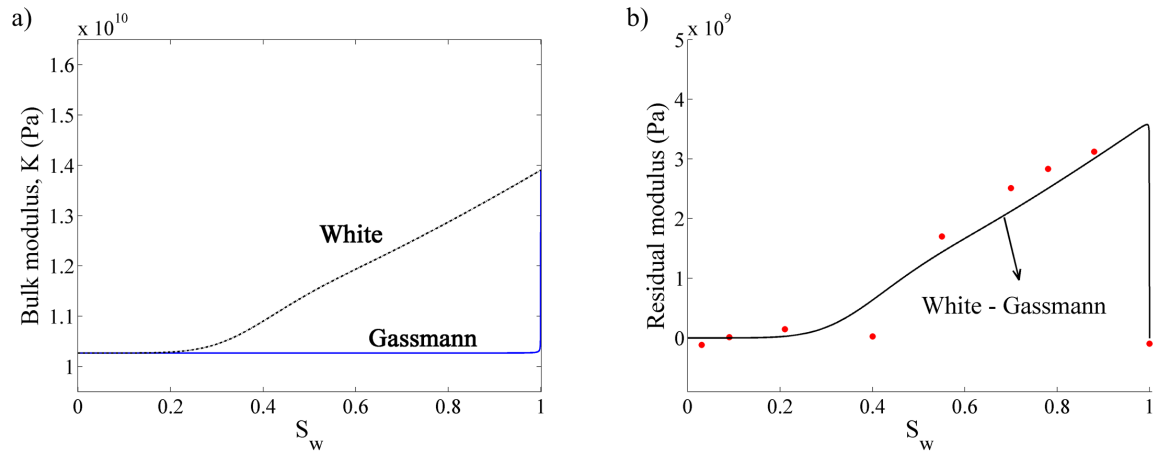


**Figure 6.** Plot showing bulk modulus predictions of White's (using a gas patch size of 0.2 mm) and Gassmann's models. (b) Subtracting Gassmann's model from White's model to obtain the dispersion due to patchy saturation and comparing to the difference between the data and the squirt model from Figure 5b.

Adding this dispersion due to patchy saturation (White's model) to the squirt model and comparing to our measured bulk modulus, we get a good fit to our experimental data (Figure 7a).
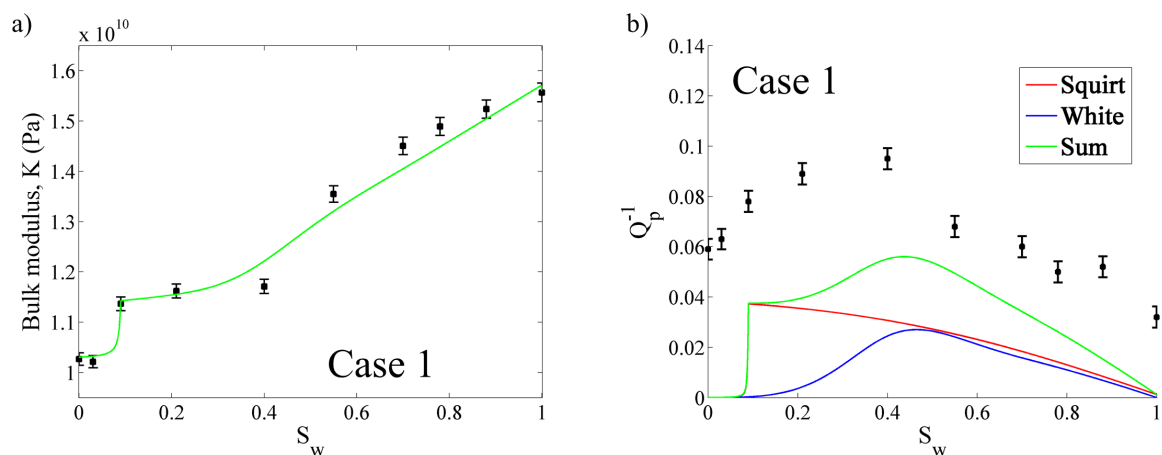
**Figure 7.** (a) Bulk modulus for the blank rock compared to the final model prediction which is obtained by summing the Squirt model (Figure 5b) and the dispersion due to patchy saturation from White's model (Figure 6b). (b) Measured attenuation compared to the resulting attenuation from the models.

The corresponding P-wave attenuation predicted from both the squirt and White models are added together and compared to our experimental data (Figure 7b). The fit is quite good, especially to the trend observed in the experiments.

**Case 2**

The second case is based on the assumption that the jump at low saturations is due to pressure discontinuity effects as described above. We start by matching the critical saturation $S_0$ where the jump occurs to the data and the magnitude of the jump at $S_0$ is fitted using the parameter "q" (Figure 8a). This wet-Gassmann model under-predicts the modulus at higher values of $S_w$ and at full water saturation as the model is consistent with Gassmann's predictions at full water saturation. We then back-out the effective fluid bulk modulus (Figure 8b) by rearranging Gassmann's equations for the fluid modulus given the saturation-dependent bulk modulus from the wet-Gassmann model. This calculated fluid bulk modulus is then placed into the model of White which we will term as the 'wet-White' (Figure 9) which also has the same full saturation (single phase) limit as Gassmann's equations.
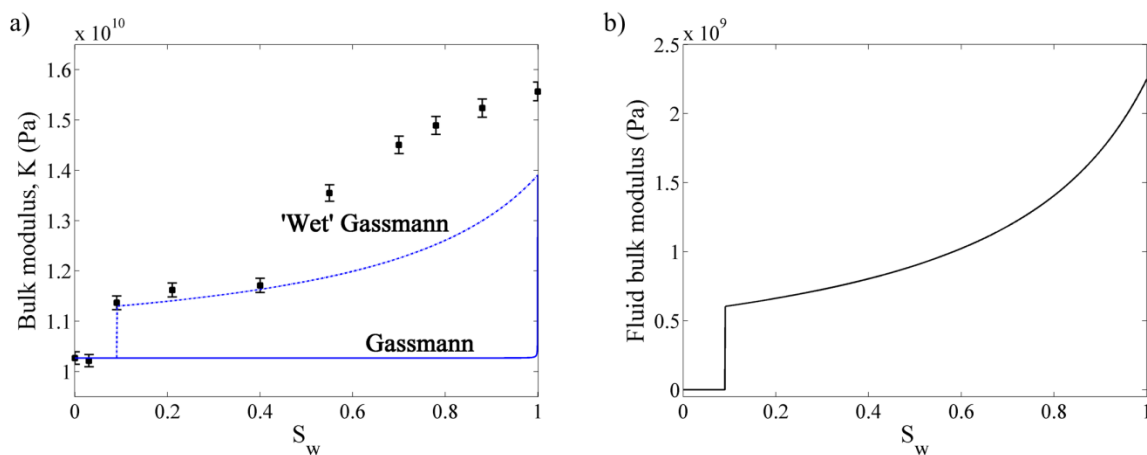
**Figure 8.** Measured bulk modulus for the blank rock compared to Gassmann's model and wet-Gassmann model. (b) Effective fluid modulus obtained from wet-Gassmann model.
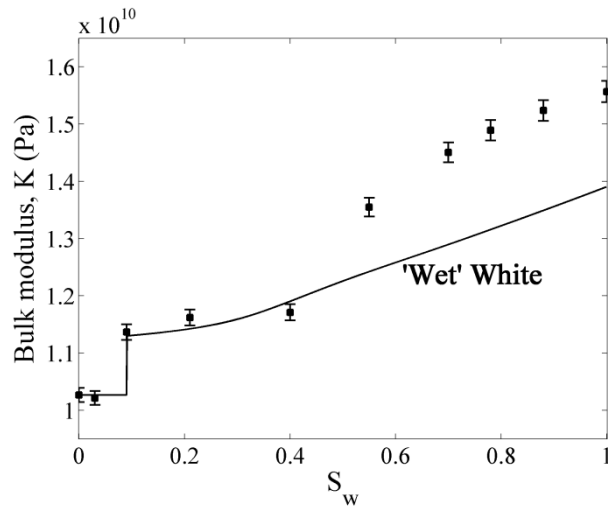


**Figure 9.** Measured bulk modulus for the blank rock compared to wet-White model.

Similar to our approach in Case 1, we subtract the experimental data from the wet White prediction to obtain the residual dispersion which we attribute to be due to squirt flow. We then fit a squirt dispersion by taking the effective fluid modulus obtained above from the wet-Gassmann model (Figure 8b) as the effective fluid in the squirt model, and then subtracting the low frequency from the high frequency squirt predictions (Figure 10a) to obtain the residual dispersion due to squirt (Figure 10b). Note that the squirt model used here is a special case of that used in Case 1 with the crack and pores assumed to have the same saturation.
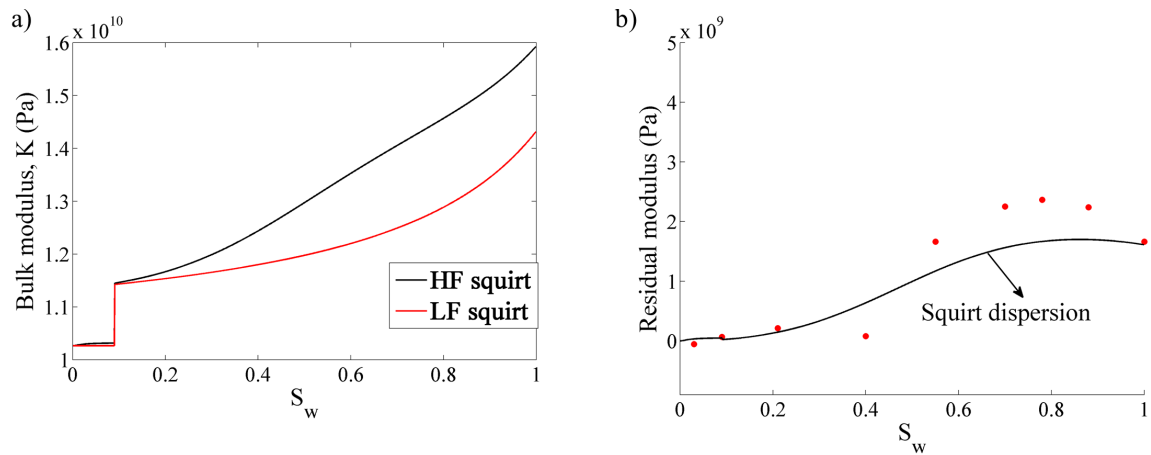
**Figure 10.** Plot showing bulk modulus predictions of the low and high frequency squirt model. (b) Subtracting the low from the high frequency model to obtain the dispersion due to squirt flow and comparing to the difference between the data and the wet-white model from Figure 9.

Adding the modelled squirt dispersion to the wet-White prediction gives us the final fit for the saturation dependence of the bulk modulus (Figure 11a). As with Case 1, the corresponding P-wave attenuation predicted from both the squirt and wet-White models are added and compared to our experimental P-wave attenuation data (Figure 11b).
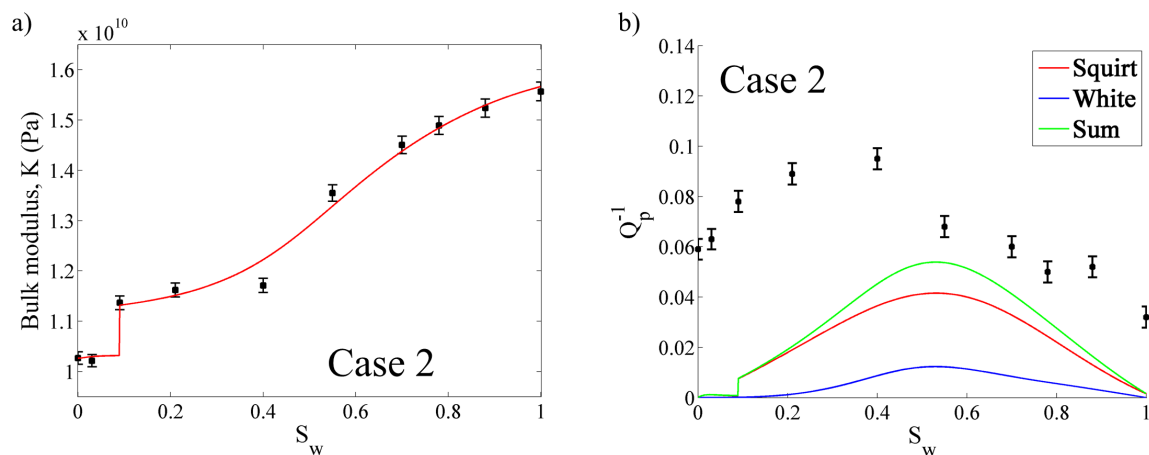


**Figure 11.** Bulk modulus for the blank rock compared to the final model prediction which is obtained by summing the wet-white model (Figure 9) and the dispersion due to squirt flow

(Figure 10b). (b) Measured attenuation compared to the resulting attenuation from the models.

| Model parameters | | | | |
|---|---|---|---|---|
| **Squirt model** | | **Blank** | **90** | **Octagonal** |
| Crack density | Case 1 | $1.35 \times 10^{-2}$ | $1.27 \times 10^{-2}$ | $1.2 \times 10^{-2}$ |
| | Case 2 | $1.75 \times 10^{-2}$ | $1.2 \times 10^{-2}$ | $1.3 \times 10^{-2}$ |
| Crack aspect ratio | | $1.0 \times 10^{-4}$ | $1.0 \times 10^{-4}$ | $1.0 \times 10^{-4}$ |
| Parameter $a$a | Case 1 | $5.0 \times 10^{-4}$ | $5.0 \times 10^{-4}$ | $5 \times 10^{-4}$ |
| | Case 2 | $2.45 \times 10^{-7}$ | $1.82 \times 10^{-7}$ | $1.0 \times 10^{-8}$ |
| **White's model** | | | | |
| Patch size | Case 1 | 1.8 mm | 1.2 mm | 0.5 mm |
| | Case 2 | 1.4 mm | 0.9 mm | 0.9 mm |
| **Wet-Gassmann model** | | | | |
| parameter q | Case 2 | 4 | 2.8 | 3.4 |

**Table 2.** Model fitting parameters obtained from nonlinear least-squares optimisation.

**Modelling results for additional samples**

We repeat the same steps for both the 90° fractured sample and the octagonal sample, and the comparisons are shown in Figures 12 and 13 for the 90° fractured sample and Figure 14 for the octagonal sample.
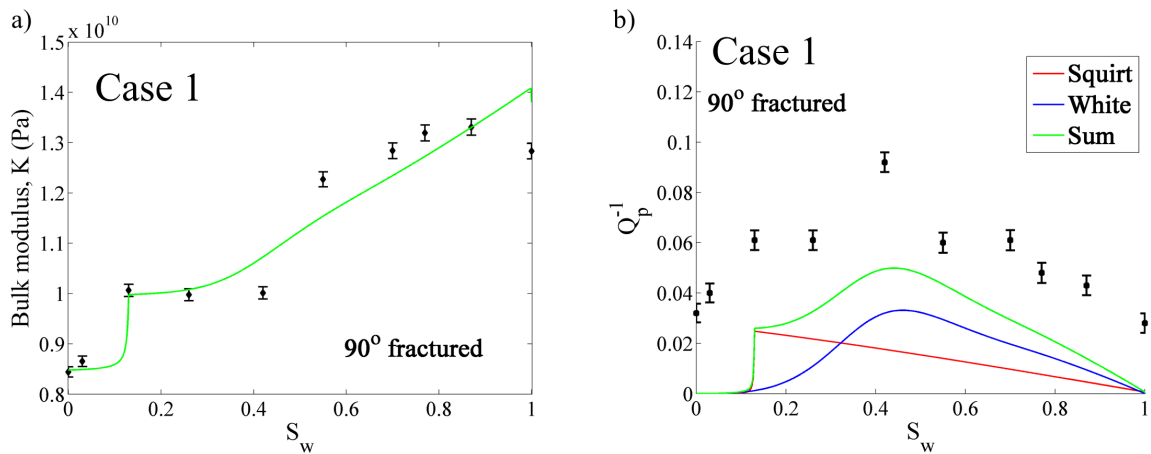


**Figure 12.** (a) Bulk modulus for the 90° fractured rock compared to the final model prediction which is obtained by summing the Squirt model prediction and the dispersion due to patchy saturation from White's model. (b) 90° fractured rock attenuation compared to the resulting attenuation from the models.
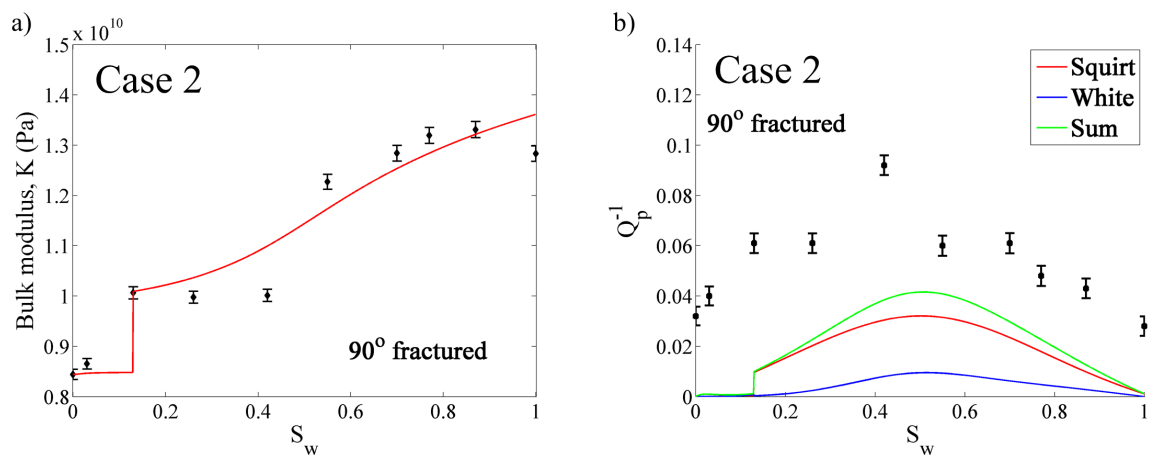


**Figure 13.** (a) Bulk modulus for the 90° fractured rock compared to the final model prediction which is obtained by summing the wet-white model and the dispersion due to

squirt flow. (b) $90^o$ fractured rock attenuation compared to the resulting attenuation from the models.
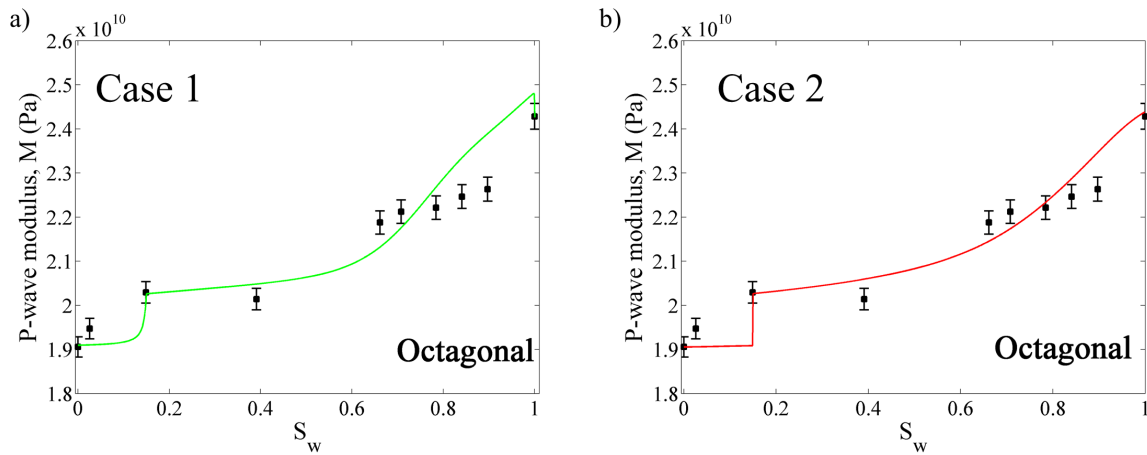


**Figure 14.** (a) P-wave modulus for the octagonal rock compared to the final model prediction which is obtained by summing the Squirt model prediction and the dispersion due to patchy saturation from White's model (case 1). (b) P-wave modulus for the octagonal rock compared to the final model prediction which is obtained by summing the wet-white model and the dispersion due to squirt flow (case 2).

### 7. Discussion

Here, we restrict our analysis to a porous rock containing two immiscible fluids having significantly different compressibilities. When a fluid such as $CO_2$ is injected into a reservoir, it dissolves over time and could become reactive, altering the rock and fluid properties but this is not considered here and neither are other chemical effects such as frame softening or swelling of clays.

The two modelling approaches presented show that different mechanisms can model the same experimental data and both produce similar results. Although the same mechanisms are used in both models (except for the wet-Gassmann model), their interpretations are different. In Case 1, the squirt effect from the cracks comes from the cracks being preferentially saturated

26

and becoming fully saturated at a critical saturation $S_0$, effectively stiffening the rock frame. This models the jump at low $S_w$ and the dispersion at $S_w = 1$. There is no additional dispersion due to squirt flow beyond $S_0$ as the cracks are fully saturated. Subsequent dispersion is as a result of patchy saturation accounted for by the model of White. In Case 2, the dispersion effect due to squirt flow does not consider the cracks to be fully saturated at $S_0$, rather the pores and cracks saturate at the same rate and dispersion due to squirt flow is observed at higher values of water saturation. However, the jump in Case 2 is modelled to be due to a discontinuous effective fluid pressure variation due to changes in capillary pressure which is a static effect as considered here. One thing that is consistent between both modelling approaches is that at full water saturation, the dispersion is due to squirt flow in agreement with previous works on dispersion in liquid saturated rocks (e.g., Chapman *et al.*, 2002, Gurevich *et al.*, 2010, Winkler, 1985).

This study supports previous suggestions that multiple mechanisms (and scales of saturation) are likely to be responsible for fluid-related effects on wave propagation in saturated porous rocks (e.g., Gist, 1994, Mavko and Nolen-Hoeksema, 1994, Müller *et al.*, 2010). No individual model or mechanism can fit the data and a combination of mechanisms is needed. This approach of combining the different models is further strengthened by the fit achieved for the attenuation data without any separate fitting. Although there are discrepancies, the trends and magnitudes as functions of water saturation show a relatively good fit. The main difference between measured and modelled attenuation can be attributed to the measured attenuation at $S_w = 0$, which is significant and unaccounted for in the models which only consider attenuation due to wave-induced fluid flow mechanisms.

The model parameters are still somewhat unconstrained; however, the relative values between samples give some insight. For example, the squirt parameter is the same for all

three samples in Case 1, indicating the high-frequency squirt limit has been reached in all three samples. The similar patch size values for Case 1 and Case 2 for each sample suggests a consistent patchy effect acting in addition to other stiffening mechanisms. It should be pointed out that the linear addition of the velocity dispersion and attenuation from different mechanisms is an approximation. However, this approach of combining attenuation and velocity dispersion due to different mechanisms has found success in previous works (Carcione *et al.*, 2012, Chichinina *et al.*, 2009) as well as in the present work.

The experimental trends presented in this paper are similar to trends presented by other investigators (Goertz and Knight, 1998, Mavko and Nolen-Hoeksema, 1994, Wulff and Burkhardt, 1997) where the trends were explained qualitatively using conceptual models of soft and stiff pores getting preferentially saturated. We present a similar mechanism using a more quantitative approach and also present a competing mechanism which has different low-frequency behaviour. We also present data on attenuation which is known to be coupled with velocity dispersion, and model the attenuation trend without having to fit the data separately.

Understanding these fluid related mechanisms require further theoretical and experimental work. A major step in this direction would be similar experiments to those presented in this work where the saturation is well controlled but conducted at lower frequencies. Many saturation experiments are carried out by injecting fluid through a pore fluid line at some position on the sample and the elastic properties measured as different amounts of fluid are injected. At low saturation values, the distribution of fluid would most likely be in the region where the fluid was injected or even possibly on the surface of the rock. This is not representative of the bulk properties of most of the pore space of the rock saturated by moisture and not representative of situations likely to occur in the subsurface where saturation occurs over a long time scale allowing enough time for capillary re-distribution of

saturation – hence a more homogeneous saturation distribution. Some other works have used drainage/drying but do not allow for capillary re-distribution of saturation and as such, at low saturations, would encounter similar problems as the injection/imbibition experiments described above. Note here that the terms imbibition and drainage are used with the assumption that the rock is water-wet and water is being injected or drained.

Experiments with image monitoring of the saturation distribution as a function of time after allowing for capillary re-distribution as discussed in the saturation methods would provide valuable insight into how important this step is for multiphase saturation experiments and what the controlling parameters are (porosity, permeability, sample size). Depending on the trends from different frequencies, we could begin to better understand these mechanisms provided the experiments are well controlled in terms of rock sample consistency and sample preparation. Synthetic rocks like those used in these experiments could help ensure sample consistency as different measurement methods usually require different sample sizes, meaning different samples have to be used. Accurate seismic monitoring of $CO_2$ saturation depends on a thorough understanding of the mechanisms for wave propagation through partially saturated rock; we believe that coupled advances in experimental and theoretical rock physics can take us towards this goal.

### 8. Conclusion

Our study demonstrates that the relationship between bulk modulus and partial saturation is complex and intrinsically involves multiple physical mechanisms. As shown in previous studies, we find that at full saturation there is evidence of rock stiffening which strongly indicates squirt flow effects. All our successful modelling attempts have required the assumption of a patchy saturated medium. Our data show an apparent jump discontinuity in the saturated bulk modulus for low saturations, and we demonstrate that this is consistent

with expected behaviour arising from pore-scale capillary effects. The interpretation is not unambiguous, however, since an alternative modelling approach based on multi-fluid squirt-flow produces similar behaviour. The two approaches both provide compelling fits to the bulk modulus and attenuation data, but their low frequency limits, which are critical for application to field data, are very different. In principle, this ambiguity could be resolved by performing the experiments over a wider frequency range.

## 9. Acknowledgments

## 10. References

Amalokwu, K., Best, A.I. & Chapman, M., 2016. Effects of aligned fractures on the response of velocity and attenuation ratios to water saturation variation: a laboratory study using synthetic sandstones, *Geophysical Prospecting,* 64**,** 942-957.

Amalokwu, K., Best, A.I., Sothcott, J., Chapman, M., Minshull, T. & Li, X.-Y., 2014. Water saturation effects on elastic wave attenuation in porous rocks with aligned fractures, *Geophysical Journal International*.

Amalokwu, K., Chapman, M., Best, A.I., Minshull, T.A. & Li, X.-Y., 2015a. Water saturation effects on P-wave anisotropy in synthetic sandstone with aligned fractures, *Geophysical Journal International,* 202**,** 1088-1095.

Amalokwu, K., Chapman, M., Best, A.I., Sothcott, J., Minshull, T.A. & Li, X.-Y., 2015b. Experimental observation of water saturation effects on shear wave splitting in synthetic rock with fractures aligned at oblique angles, *Geophysical Journal International,* 200**,** 17-24.

Arts, R., Eiken, O., Chadwick, A., Zweigel, P., van der Meer, L. & Zinszner, B., 2004. Monitoring of CO2 injected at Sleipner using time-lapse seismic data, *Energy,* 29**,** 1383-1392.

Best, A.I., Sothcott, J. & McCann, C., 2007. A laboratory study of seismic velocity and attenuation anisotropy in near-surface sedimentary rocks, *Geophysical Prospecting,* 55**,** 609-625.

Biot, M.A., 1956. Theory of propagation of elastic waves in fluid-saturated porous solid, I. Low frequency range, II. Higher frequency range, *J. of the Acous. Soc. of America,* 28**,** 168-191.

Brie, A., Pampuri, F., Marsala, A. & Meazza, O., 1995. Shear sonic interpretation in gas-bearing sands. *in SPE Annual Technical Conference and Exhibition.*

Cadoret, T., Marion, D. & Zinszner, B., 1995. Influence of frequency and fluid distribution on elastic wave velocities in partially saturated limestones, *Journal of Geophysical Research: Solid Earth,* 100**,** 9789-9803.

Carcione, J., Helle, H. & Pham, N., 2003. White's model for wave propagation in partially saturated rocks: Comparison with poroelastic numerical experiments, *GEOPHYSICS,* 68**,** 1389-1398.

Carcione, J.M., Cavallini, F., Santos, J.E., Ravazzoli, C.L. & Gauzellino, P.M., 2004. Wave propagation in partially saturated porous media: simulation of a second slow wave, *Wave Motion,* 39**,** 227-240.

Carcione, J.M., Santos, J.E. & Picotti, S., 2012. Fracture-Induced Anisotropic Attenuation, *Rock Mechanics and Rock Engineering,* 45**,** 929-942.

Castagna, J.P., Sun, S. & Siegfried, R.W., 2003. Instantaneous spectral analysis: Detection of low-frequency shadows associated with hydrocarbons, *The Leading Edge,* 22**,** 120-127.

Chadwick, A., Williams, G., Delepine, N., Clochard, V., Labat, K., Sturton, S., Buddensiek, M.-L., Dillen, M., Nickel, M., Lima, A.L., Arts, R., Neele, F. & Rossi, G., 2010. Quantitative analysis of time-lapse seismic monitoring data at the Sleipner CO2 storage operation, *The Leading Edge,* 29**,** 170-177.

Chapman, M., 2003. Frequency-dependent anisotropy due to meso-scale fractures in the presence of equant porosity, *Geophysical Prospecting,* 51**,** 369-379.

Chapman, M., Zatsepin, S.V. & Crampin, S., 2002. Derivation of a microstructural poroelastic model, *Geophysical Journal International,* 151**,** 427-451.

Chichinina, T., Obolentseva, I., Gik, L., Bobrov, B. & Ronquillo-Jarillo, G., 2009. Attenuation anisotropy in the linear-slip model: Interpretation of physical modeling data, *GEOPHYSICS,* 74**,** WB165-WB176.

Domenico, S.N., 1976. Effect of brine-gas mixture on velocity in an unconsolidated sand reservoir, *Geophysics,* 41**,** 882-894.

Dutta, N.C. & Seriff, A.J., 1979. On White's model of attenuation in rocks with partial gas saturation, *Geophysics,* 44**,** 1806-1812.

Eid, R., Ziolkowski, A., Naylor, M. & Pickup, G., 2015. Seismic monitoring of CO2 plume growth, evolution and migration in a heterogeneous reservoir: Role, impact and importance of patchy saturation, *International Journal of Greenhouse Gas Control,* 43**,** 70-81.

Endres, A.L. & Knight, R., 1991. The effects of pore-scale fluid distribution on the physical properties of partially saturated tight sandstones, *Journal of Applied Physics,* 69**,** 1091-1098.

Endres, A.L. & Knight, R.J., 1997. Incorporating pore geometry and fluid pressure communication into modeling the elastic behavior of porous rocks, *GEOPHYSICS,* 62**,** 106-117.

Falcon-Suarez, I., North, L., Amalokwu, K. & Best, A., 2016. Integrated geophysical and hydromechanical assessment for CO2 storage: shallow low permeable reservoir sandstones, *Geophysical Prospecting,* 64**,** 828-847.

Gassmann, F., 1951. Elasticity of porous media, *Vierteljahrsschrder Naturforschenden Gesselschaft,* 96**,** 1-23.

Ghosh, R., Sen, M.K. & Vedanti, N., 2015. Quantitative interpretation of CO2 plume from Sleipner (North Sea), using post-stack inversion and rock physics modeling, *International Journal of Greenhouse Gas Control,* 32**,** 147-158.

Gist, G.A., 1994. Interpreting laboratory velocity measurements in partially gas-saturated rocks, *Geophysics,* 59**,** 1100-1109.

Goertz, D. & Knight, R., 1998. Elastic wave velocities during evaporative drying, *GEOPHYSICS,* 63**,** 171-183.

Greenspan, L., 1977. Humidity Fixed Points of Binary Saturated Aqueous Solutions, *J. Res. Nat. Bur. Stand. (U.S.) - A (Phys. And Chem.),* 81A**,** 89-96.

Gregory, A., 1976. FLUID SATURATION EFFECTS ON DYNAMIC ELASTIC PROPERTIES OF SEDIMENTARY ROCKS, *Geophysics,* 41**,** 895-921.

Gurevich, B., Makarynska, D., de Paula, O.B. & Pervukhina, M., 2010. A simple model for squirt-flow dispersion and attenuation in fluid-saturated granular rocks, *Geophysics,* 75**,** N109-N120.

Johnson, K.L., Kendall, K. & Roberts, A.D., 1971. Surface Energy and the Contact of Elastic Solids, *Proceedings of the Royal Society of London. A. Mathematical and Physical Sciences,* 324**,** 301-313.

King, M.S., Marsden, J.R. & Dennis, J.W., 2000. Biot dispersion for P- and S-wave velocities in partially and fully saturated sandstones, *Geophysical Prospecting,* 48**,** 1075-1089.

Knight, R., Dvorkin, J. & Nur, A., 1998. Acoustic signatures of partial saturation, *GEOPHYSICS,* 63**,** 132-138.

Krevor, S., Blunt, M.J., Benson, S.M., Pentland, C.H., Reynolds, C., Al-Menhali, A. & Niu, B., 2015. Capillary trapping for geologic carbon dioxide storage – From pore scale physics to field scale implications, *International Journal of Greenhouse Gas Control,* 40**,** 221-237.

Lebedev, M., Pervukhina, M., Mikhaltsevitch, V., Dance, T., Bilenko, O. & Gurevich, B., 2013. An experimental study of acoustic responses on the injection of supercritical CO2 into sandstones from the Otway Basin, *GEOPHYSICS,* 78**,** D293-D306.

Lei, X. & Xue, Z., 2009. Ultrasonic velocity and attenuation during CO2 injection into water-saturated porous sandstone: Measurements using difference seismic tomography, *Physics of the Earth and Planetary Interiors,* 176**,** 224-234.

Marion, D. & Jizba, D., 1992. Acoustic properties and their dependence on porosity, mineralogy and saturation: Applications to field-scale measurements. *in Third European Core Analysis Symposium Soc. of Core AnalParis.*

Mavko, G., Mukerji, T. & Dvorkin, J., 2009. *The Rock Physics Handbook,* edn, Vol., pp. Pages, Cambridge University Press.

Mavko, G. & Nolen-Hoeksema, R., 1994. Estimating seismic velocities at ultrasonic frequencies in partially saturated rocks, *GEOPHYSICS,* 59**,** 252-258.

McCann, C. & Sothcott, J., 1992. Laboratory measurements of the seismic properties of sedimentary rocks, *Geological Society, London, Special Publications,* 65**,** 285-297.

Müller, T., Gurevich, B. & Lebedev, M., 2010. Seismic wave attenuation and dispersion resulting from wave-induced flow in porous rocks — A review, *GEOPHYSICS,* 75**,** 75A147-175A164.

Murphy, W., Winkler, K. & Kleinberg, R., 1986. Acoustic relaxation in sedimentary rocks: Dependence on grain contacts and fluid saturation, *Geophysics,* 51**,** 757-766.

Murphy, W.F., 1982. Effects of partial water saturation on attenuation in Massillon sandstone and Vycor porous glass, *J. Acoust Soc. Am.,* 71**,** 1458–1468.

Murphy, W.F., 1984. Acoustic measures of partial gas saturation in tight sandstones, *Journal of Geophysical Research: Solid Earth,* 89**,** 11549-11559.

Murphy, W.F., 1985. Sonic and ultrasonic velocities: Theory Versus experiment, *Geophysical Research Letters,* 12**,** 85-88.

Nakagawa, S., Kneafsey, T.J., Daley, T.M., Freifeld, B.M. & Rees, E.V., 2013. Laboratory seismic monitoring of supercritical CO2 flooding in sandstone cores using the Split Hopkinson Resonant Bar technique with concurrent x-ray Computed Tomography imaging, *Geophysical Prospecting,* 61**,** 254-269.

Paffenholz, J. & Burkhardt, H., 1989. Absorption and modulus measurements in the seismic frequency and strain range on partially saturated sedimentary rocks, *Journal of Geophysical Research: Solid Earth,* 94**,** 9493-9507.

Papageorgiou, G., Amalokwu, K. & Chapman, M., 2016. Theoretical derivation of a Brie-like fluid mixing law, *Geophysical Prospecting,* 64**,** 1048-1053.

Papageorgiou, G. & Chapman, M., 2015. Multifluid squirt flow and hysteresis effects on the bulk modulus–water saturation relationship, *Geophysical Journal International,* 203**,** 814-817.

Papamichos, E., Brignoli, M. & Santarelli, F.J., 1997. An experimental and theoretical study of a partially saturated collapsible rock, *Mechanics of Cohesive-frictional Materials,* 2**,** 251-278.

Santos, J.E., Corberó, J.M. & Douglas, J., 1990. Static and dynamic behavior of a porous solid saturated by a two-phase fluid, *The Journal of the Acoustical Society of America,* 87**,** 1428-1438.

Schmitt, L., Forsans, T. & Santarelli, F.J., 1994. Shale testing and capillary phenomena, *Int. J. Rock Mech. Min. Sci. & Geomech. Abstr.,* 31**,** 411 – 427.

Shi, J.-Q., Xue, Z. & Durucan, S., 2007. Seismic monitoring and modelling of supercritical $CO_2$ injection into a water-saturated sandstone: Interpretation of P-wave velocity data, *International Journal of Greenhouse Gas Control,* 1**,** 473-480.

Thomsen, L., 1995. Elastic anisotropy due to aligned cracks in porous rock, *Geophysical Prospecting* 43**,** 805-829.

Tillotson, P., Chapman, M., Sothcott, J., Best, A.I. & Li, X.-Y., 2014. Pore fluid viscosity effects on P- and S-wave anisotropy in synthetic silica-cemented sandstone with aligned fractures, *Geophysical Prospecting,* 62**,** 1238-1252.

Tillotson, P., Sothcott, J., Best, A.I., Chapman, M. & Li, X.-Y., 2012. Experimental verification of the fracture density and shear-wave splitting relationship using synthetic silica cemented sandstones with a controlled fracture geometry, *Geophysical Prospecting,* 60**,** 516-525.

Toms, J., Müller, T.M. & Gurevich, B., 2007. Seismic attenuation in porous rocks with random patchy saturation, *Geophysical Prospecting,* 55**,** 671-678.

Walsh, J.B., 1995. Seismic attenuation in partially saturated rock, *Journal of Geophysical Research: Solid Earth,* 100**,** 15407-15424.

White, J.E., 1975. Computed seismic speeds and attenuation in rocks with partial gas saturation, *Geophysics,* 40**,** 224-232.

Winkler, K., 1985. Dispersion analysis of velocity and attenuation in Bera Sandstone, *Journal of Geophysical Research,* 90**,** 6793-6800.

Winkler, K. & Nur, A., 1982. Seismic attenuation: Effects of pore fluids and frictional-sliding, *GEOPHYSICS,* 47**,** 1-15.

Winkler, K.W. & Murphy, W.F., 1995. Acoustic velocity and attenuation in porous rocks, *Rock Physics and Phase Relations,* 3**,** 20-34.

Wu, X., Chapman, M., Li, X.-Y. & Boston, P., 2014. Quantitative gas saturation estimation by frequency-dependent amplitude-versus-offset analysis, *Geophysical Prospecting,* 62**,** 1224-1237.

Wulff, A.M. & Burkhardt, H., 1997. Mechanisms affecting ultrasonic wave propagation in fluid-containing sandstones under high hydrostatic pressure, *Journal of Geophysical Research: Solid Earth,* 102**,** 3043-3050.

Zhang, Z.F., Oostrom, M. & White, M.D., 2016. Relative permeability for multiphase flow for oven-dry to full saturation conditions, *International Journal of Greenhouse Gas Control,* 49**,** 259-266.

## A. Appendix

Gassmann's formula gives the bulk modulus $K$ of a porous matrix of porosity $\phi$ with mineral modulus $K_m$, dry modulus $K_d$ and fluid modulus $K_f$:

$$K = K_d + \frac{\left(1 - \frac{K_d}{K_m}\right)^2}{\frac{\phi}{K_f} + \frac{(1-\phi)}{K_m} - \frac{K_d}{K_m^2}} \qquad \text{A-1}$$

White's model considers spherical gas-filled regions of radius $a$ located periodically at the centre of a liquid-filled cubic array in a porous rock. For simplicity, White considered a unit cell where the liquid-filled cube is replaced with a sphere of radius $b$ and the inner gas-filled sphere has a radius of $a$ ($b > a$) so that the gas saturation is given as $S_g = (a/b)^3$. The complex bulk modulus $K^*$ (accounting for a correction pointed out by Dutta and Seriff (1979)) is given as (Mavko *et al.*, 2009):

$$K^* = \frac{K_\infty}{1 - K_\infty W}, \qquad \text{A-2}$$

where

$$W = \frac{3a^2(R_1 - R_2)(-Q_1 + Q_2)}{b^3 i\omega(Z_1 + Z_2)}$$

$$R_1 = \frac{K_1 - K_d}{1 - K_d/K_m} \frac{3K_2 + 4\mu_d}{K_2(3K_1 + 4\mu_d) + 4\mu_d(K_1 - K_2)S_g}$$

$$R_2 = \frac{K_2 - K_d}{1 - K_d/K_m} \frac{3K_1 + 4\mu_d}{K_2(3K_1 + 4\mu_d) + 4\mu_d(K_1 - K_2)S_g}$$

$$Z_1 = \frac{\eta_1 a}{\kappa_1} \left[ \frac{1 - e^{-2\alpha_1 a}}{(\alpha_1 a - 1) + (\alpha_1 a + 1)e^{-2\alpha_1 a}} \right] \qquad \text{A-3}$$

$$Z_2 = -\frac{\eta_2 a}{\kappa_2} \left[ \frac{(\alpha_2 b + 1) + (\alpha_2 b - 1)e^{2\alpha_2(b-a)}}{(\alpha_2 b + 1)(\alpha_2 a - 1) - (\alpha_2 b - 1)(\alpha_2 a + 1)e^{2\alpha_2(b-a)}} \right],$$

where

$$\alpha_j = (i\omega\eta_j/\kappa_j K_{Ej})^{1/2}$$

$$K_{Ej} = \left[ 1 - \frac{K_{fj}(1 - K_j/K_m)(1 - K_d/K_m)}{\phi K_j(1 - K_{fj}/K_m)} \right] K_{Aj}$$

$$K_{Aj} = \left( \frac{\phi}{K_{fj}} + \frac{1 - \phi}{K_m} - \frac{K_d}{K_m^2} \right)^{-1}$$

$$Q_j = \frac{(1 - K_d/K_m)K_{Aj}}{K_j}. \qquad \text{A-4}$$

$$K_\infty = \frac{K_2(3K_1 + 4\mu_d) + 4\mu_d(K_1 - K_2)S_g}{(3K_1 + 4\mu_d) - 3(K_1 - K_2)S_g}, \qquad \text{A-5}$$

Here, in addition to the terms in Gassmann's formula, $\mu_d$ represents the dry rock shear modulus, $j = 1 \ or \ 2$ represents parameters relating to the two different regions of the unit cell. The subscripts 1 and 2 refer the inner region and outer region, respectively. $K_j$ and $\mu_j$ are saturated bulk and shear moduli obtained by saturating the dry rock moduli with fluid 1 and 2 using Gassmann's equation. Note the shear moduli is not affected by saturation in the models of White and Gassmann so that $\mu_j = \mu_d$.

Papageorgiou and Chapman's bulk modulus written as a functions of the dry rock bulk modulus $K_d$, and corrections from the cracks and pores (represented by superscripts $c$ and $p$ respectively) is given as (Papageorgiou and Chapman, 2015):

$$K_{eff} = K_d - \phi_0^c \left(\frac{K_m}{\sigma_c} + 1\right) \frac{\alpha B_1 (\beta A_2 + 1) + \beta B_2}{1 - (\alpha A_1 + 1)(\beta A_2 + 1)}$$

$$- \phi_0^p \left(\frac{3K_m}{4\mu} + 1\right) \frac{\beta B_2 (\alpha A_1 + 1) + \alpha B_1}{1 - (\alpha A_1 + 1)(\beta A_2 + 1)},$$

A-6

where

$$\alpha = i\frac{\phi_0^c \omega}{\sigma_c \zeta} \frac{\tilde{\eta}}{\tilde{k}} \qquad \beta = i\frac{3\phi_0^p \omega}{4\mu \zeta} \frac{\tilde{\eta}}{\tilde{k}}$$

$$A_1 = 1 + \frac{\sigma_c}{K_-} \qquad A_2 = 1 + \frac{4\mu}{3K_+}$$

A-7

$$B_1 = K_m \qquad B_2 = 3K_m \frac{1 - \nu}{1 + \nu}.$$